# Intraseasonal Forecasting of the Asian Summer Monsoon in Four Operational and Research Models*

XIOUHUA FU, JUNE-YI LEE, AND BIN WANG

*IPRC, SOEST, University of Hawaii at Manoa, Honolulu, Hawaii*

WANQIU WANG

*Climate Prediction Center, National Centers for Environmental Prediction, Camp Spring, Maryland*

FREDERIC VITART

*European Centre for Medium-Range Weather Forecasts, Reading, United Kingdom*

(Manuscript received 4 May 2012, in final form 11 December 2012)

ABSTRACT

The boreal summer intraseasonal oscillation (BSISO) is a dominant tropical mode with a period of 30–60 days, which offers an opportunity for intraseasonal forecasting of the Asian summer monsoon. The present study provides a preliminary, yet up-to-date, assessment of the prediction skill of the BSISO in four state-of-the-art models: the ECMWF model, the University of Hawaii (UH) model, the NCEP Climate Forecast System, version 2 (CFSv2), and version 1 for the 2008 summer (CFSv1), which is a common year of two international programs: the Year of Tropical Convection (YOTC) and Asian Monsoon Years (AMY). The mean prediction skill over the global tropics and Southeast Asia for first three models reaches about 1–2 (3) weeks for BSISO-related rainfall (850-hPa zonal wind), measured as the lead time when the spatial anomaly correlation coefficient drops to 0.5. The skill of CFSv1 is consistently lower than the other three. The strengths and weaknesses of the CFSv2, UH, and ECMWF models in forecasting the BSISO for this specific year are further revealed. The ECMWF and UH have relatively better performance for northward-propagating BSISO when the initial convection is near the equator, although they suffer from an early false BSISO onset when initial convection is in the off-equatorial monsoon trough. However, CFSv2 does not have a false onset problem when the initial convection is in monsoon trough, but it does have a problem with very slow northward propagation. After combining the forecasts of CFSv2 and UH into an equal-weighted multimodel ensemble, the resultant skill is slightly better than that of individual models. An empirical model shows a comparable skill with the dynamical models. A combined dynamical–empirical ensemble advances the intraseasonal forecast skill of BSISO-related rainfall to three weeks.

## 1. Introduction

Every year, the Asian summer monsoon brings much-needed water into South and East Asia from the Indo–Pacific Ocean to sustain more than 60% of the world's population living on this biggest continent on Earth. On the other hand, the Asian summer monsoon exhibits rich variability with a wide range of time scales from synoptic (~days) and intraseasonal (~weeks) to interannual (~years) and beyond, which makes efficient water management, agricultural planning, and disaster prevention very difficult. For the well-being of the societies affected by the monsoon, the capability of forecasting the Asian monsoon systems with lead times from days and weeks to years and beyond is very desirable.

Medium-range weather forecasts with a lead time of one week (Lorenz 2006) have been routinely carried out by all national weather services around the world for decades. Seasonal prediction, based on the premise that

* School of Ocean and Earth Science and Technology Contribution Number 8898 and International Pacific Research Center Contribution Number 963.

*Corresponding author address:* Dr. Joshua Xiouhua Fu, IPRC, SOEST, University of Hawaii at Manoa, 1680 East–West Road, POST Bldg. 409D, Honolulu, HI 96822.
E-mail: xfu@hawaii.edu

DOI: 10.1175/JCLI-D-12-00252.1

there is long-range forecasting memory residing in underlying boundary conditions (e.g., SST, soil moisture, sea ice, etc.), has also been launched by a large number of operational and research centers around the world since the late 1980s (Cane et al. 1986; Shukla 1998; B. Wang et al. 2009; Shukla et al. 2009; Lee et al. 2010). An obvious forecasting gap exists between weather forecast and seasonal prediction. The recurrent nature of tropical intraseasonal variability with a period of 30–60 days offers a golden opportunity to fill this gap (Waliser et al. 2003). However, the current modeling and forecasting capability of tropical intraseasonal variability and its influence on the Asian summer monsoon is still very limited (Lin et al. 2006; Fu et al. 2007; Matsueda and Endo 2011), although much research has been conducted intending to address this issue since early 1970s (Madden and Julian 1971; Krishnamurti 1971; Lau and Waliser 2012).

In boreal summer, tropical intraseasonal variability initiates over the western Indian Ocean and propagates both northward and eastward (Yasunari 1979; Wang and Rui 1990; Fu et al. 2003; Lee et al. 2013). On its passage, the tropical intraseasonal variability modulates the occurrence of monsoon depressions and tropical cyclones in the northern Indian Ocean (Goswami et al. 2003; Kikuchi et al. 2009), South China Sea, and western North Pacific Ocean (Nakazawa 1986; Liebmann et al. 1994; Chen and Weng 1999). After reaching the Asian continent, tropical intraseasonal variability brings active and break spells to the Asian summer monsoon. The tropical intraseasonal variability in northern summer is also known as the monsoon intraseasonal oscillation (MISO; Hoyos and Webster 2007) or more generally as the boreal summer intraseasonal oscillation (BSISO; Wang and Xie 1997).

In an intuitive sense, the oscillating nature of the BSISO offers an upper limit of predictability of about two months (van den Dool and Saha 1990). Using 23-yr intraseasonal-filtered daily all-Indian rainfall, Goswami and Xavier (2003) assessed the predictability of BSISO-related rainfall to be about 20 and 10 days, respectively, for break and active monsoon phases, which suggested that the active-to-break monsoon transition is more predictable than the break-to-active transition. The latter transition represents a ''monsoon prediction barrier.'' Using 30-yr intraseasonal-filtered daily outgoing longwave radiation (OLR) observations with a different method, Ding et al. (2011) assessed the potential predictability of the BSISO to be about 35 days. The assessment with several atmospheric general circulation models indicated that the dynamical variables of the BSISO have much longer predictability than the convective variables (Waliser et al. 2003; Liess et al. 2005; Reichler and Roads 2005). Fu et al. (2007) demonstrated that the inclusion of two-way air–sea interactions in a University of Hawaii (UH) model[1] extends the BSISO predictability in the atmosphere-only version by at least one week. The resultant potential predictability of BSISO-related rainfall in the UH model reaches around 40 days (Fu et al. 2008).

The forecast skill of the BSISO, however, is still much shorter than its potential predictability as a result of model weaknesses in accurately representing the initiation, structure, intensity, and propagation of the BSISO; errors existing in the initial and boundary conditions; and the misrepresentation of atmosphere–ocean interactions (Chen and Alpert 1990; Lau and Chang 1992; Hendon et al. 2000; Seo et al. 2005; Woolnough et al. 2007; Vitart et al. 2007; Fu et al. 2009; Fu et al. 2011). The pioneering study of Krishnamurti et al. (1992) suggested that the useful skill of the flow fields of the BSISO could reach 20–30 days in several cases. The forecast skill of an older version (Hendon et al. 2000; Jones et al. 2000) and an updated version (Seo et al. 2005) of the National Centers for Environmental Prediction (NCEP) forecast model, however, was only about one week for the BSISO-related dynamic fields. After improving model physics (e.g., Bechtold et al. 2008; Seo et al. 2009) and using latest-generation reanalysis datasets [e.g., Climate Forecast System Reanalysis (CFSR), Modern-Era Retrospective Analysis for Research and Applications (MERRA), and the European Centre for Medium-Range Weather Forecasts (ECMWF) Interim Re-Analysis (ERA-Interim)] as initial conditions (Saha et al. 2010; Rienecker et al. 2009; Simmons et al. 2007), intraseasonal forecasting skills have shown significant advancement in recent years (Vitart and Molteni 2009; Rashid et al. 2011; Fu et al. 2011; Zhang and van den Dool 2012).

In this study, we extend our previous work (Fu et al. 2011) to include more models: the ECMWF model, the NCEP Climate Forecast System, versions 1 and 2 (CFSv1 and CFSv2); and the UH research model. The objectives of this study are threefold: 1) to provide a preliminary, yet up-to-date, assessment of intraseasonal forecast skill for these four models in summer 2008, which is a common year of two international programs: the Year of Tropical Convection (YOTC; http://www.ucar.edu/yotc/) (Waliser et al. 2012) and the Asian Monsoon Years (AMY; http://www.wcrp-amy.org/); 2) to identify the strengths and weaknesses of individual models on intraseasonal forecast

[1] This model coupled a modified ECHAM4 atmospheric general circulation model with an intermediate upper-ocean model developed at University of Hawaii. For simplicity, this coupled model is referred to as the UH model.

of the BSISO, which will provide useful insights for further model evaluation and improvement; and 3) to explore ways to advance the intraseasonal forecast skill of the BSISO—for example, through the developments of a multimodel ensemble and a combined dynamical–empirical ensemble. The remaining parts of this paper are organized as follows. Section 2 describes the models used to produce the forecasts and methods used to measure the forecast skill. Section 3 documents the intraseasonal forecast skill of the four models over the global tropics and reveals the strengths and weaknesses of individual models in this specific year. In section 4, we focus on the intraseasonal forecasting of the monsoon over Southeast Asia and also analyze the phase dependences of monsoon forecast skills. In the last section, we discuss possible causes of the individual models' weaknesses and explore the potential of multimodel and dynamical–empirical approaches on the advancement of intraseasonal forecasting, and summarize our major findings.

## 2. Models and methods

The four models used in this study are briefly described in this section. The details of individual models can be found in given references. The atmospheric component of the ECMWF monthly system (Vitart et al. 2008) is a version of the ECMWF Integrated Forecast System (IFS) known as cycle 36r2 (operational in 2011) with a horizontal resolution of T639 (about 30 km). The ECMWF monthly system runs in an atmosphere-only mode during the first 10 days forced with persistent SST. After 10 days, the system runs in a coupled mode with the atmospheric model resolution reduced to T319 (about 60 km); the ocean component is a general circulation model, the Hamburg Ocean Primitive Equation (HOPE; Wolff et al. 1997). The resolution change of the atmospheric model is expected to have little impact on the simulation of intraseasonal variability (Jung et al. 2012). In total, 51 ensemble forecasts covering one month were generated by the ECMWF model and initialized weekly with the ERA-Interim (Simmons et al. 2007). From each week's forecasts, 5 out of a total of 51 ensembles were randomly selected and used in this study. Because the ensemble spread of the ECMWF forecasts is modest on the intraseasonal time scale (the ensemble spread of ECMWF forecasts can be found online at http://www.cpc.ncep.noaa.gov/products/precip/CWlink/MJO/CLIVAR/clivar_wh.shtml), the mean of five random ensembles can be viewed as a good representative of the model's overall performance (F. Vitart 2011, personal communication).

In August 2004, CFSv1 became operational at NCEP. Saha et al. (2006) documented the details of this system and its performance on seasonal prediction. The atmospheric component of CFSv1 is the NCEP atmospheric Global Forecast System (GFS) model with a horizontal resolution of T62 (about 200 km), which has represented the version since February 2003 (Moorthi et al. 2011). The oceanic component of CFSv1 is the Geophysical Fluid Dynamics Laboratory (GFDL) Modular Ocean Model, version 3 (MOM3; Pacanowski and Griffies 1998). Daily season-long forecasts have been routinely carried out with CFSv1 using the NCEP–Department of Energy (DOE) Reanalysis 2 (R2) as initial conditions. The CFSv2 model is the latest-generation climate forecast system at NCEP, which became operational in March 2011. The atmospheric component is the frozen version of the GFS as of May 2010 with a horizontal resolution of T126 (about 100 km). The ocean component has been upgraded to MOM4. The CFSv2 model includes a more comprehensive land and sea ice model. A new-generation reanalysis (CFSR) has been generated with CFSv2 (Saha et al. 2010). Daily season-long retrospective forecasts back to 1982 have been produced with CFSv2 initialized with CFSR. For both CFSv1 and CFSv2, the forecasts initialized four times (0000, 0600, 1200, and 1800 UTC) each day are treated as four ensembles. Their daily ensemble mean was used in this study.

The UH model is an atmosphere–ocean coupled model (Fu et al. 2003) developed at the University of Hawaii. The atmospheric component is a general circulation model (ECHAM4) with a T106 (about 125 km) resolution that was originally developed at the Max Planck Institute for Meteorology, Germany (Roeckner et al. 1996). The mass flux scheme of Tiedtke (1989) is used to represent deep, shallow, and midlevel convections. The ocean component is an intermediate upper-ocean model developed at UH. It comprises a mixed layer and a thermocline layer with a horizontal resolution of $0.5° \times 0.5°$. Ten ensemble 45-day forecasts for summer 2008 have been carried out with the UH model every 10 days initialized with a final operational global analysis at $1° \times 1°$ produced by NCEP (also known as FNL; more details can be found online at http://dss.ucar.edu/datasets/ds083.2). Ten initial ensemble conditions are generated by simply adding day-to-day differences to the unperturbed initial condition, which is the FNL analysis in this study.

To assess the intraseasonal forecast skills, 120-day observations (Tropical Rainfall Measuring Mission rainfall and 850-hPa zonal winds from the FNL analysis) before the initial dates have been concatenated to the 30-day (or 45 day) ensemble-mean forecasts along with several months' zero padded in the end. The merged time series are bandpass filtered to extract intraseasonal variability (30–90 days) from the forecasts. In a similar fashion, the observed intraseasonal variability is also extracted. The

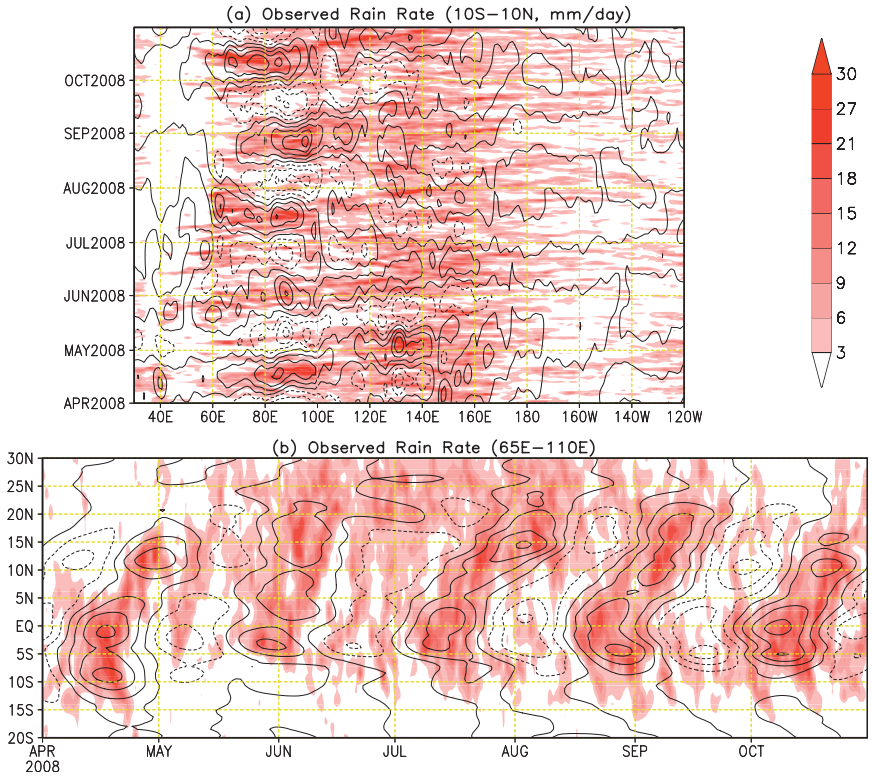


FIG. 1. Observed (a) time–longitude (averaged over 10°S–10°N) and (b) latitude–time (averaged over 65°–110°E) evolutions of rainfall rate (shading; mm day$^{-1}$) and 30–90-day-filtered monsoon intraseasonal oscillations [contours; contour interval (CI) is 2 mm day$^{-1}$] in the summer 2008. Solid (dashed) contours represent positive (negative) anomalies.

efficiency of this method of extracting intraseasonal variability has been demonstrated in Wheeler and Weickmann (2001). Finally, the spatial anomaly correlation coefficients (ACCs) and root-mean-square errors (RMSEs) between the forecasted and observed intraseasonal anomalies are calculated during the forecast period (Wilks 2005), respectively, for the global tropics (30°S–30°N) and Southeast Asia (10°–30°N, 60°–120°E).

## 3. Intraseasonal forecast skill over the global tropics

### *a. Intercomparison of seasonal-mean skill*

As previously mentioned, 2008 is a target year of YOTC and AMY (Waliser et al. 2012). One of the common goals of these two international weather and climate programs is to assess and improve the intraseasonal forecast capability over the global tropics, particularly for the Asian summer monsoon. The temporal evolution of observed rainfall along the equator in the summer 2008 is shown in Fig. 1a. Five intraseasonal events occurred during this summer. Four of them moved eastward; one event in July moved westward. The two in April and October significantly weaken when crossing the Maritime Continent. The other two in May and August, however, propagate smoothly over the Maritime Continent. Although all five events propagate northward from near the equator into South and East Asia (Fig. 1b), the event in late May and early June propagates much faster than other four events. These interevent differences highlight the intermittent nature of tropical intraseasonal variability (Goulet and Duvel 2000; Matthews 2008) and also pose a great challenge for intraseasonal forecasting of the monsoon.

The seasonal-mean intraseasonal forecast skills of global tropical rainfall and 850-hPa zonal wind (U850 hereafter) in the summer 2008 for the four models are shown in Fig. 2. Instead of using a modest ACC criterion of 0.4 as in Fu et al. 2011, we define the forecast lead time as when ACC drops to 0.5 as the forecast skill in this study. Figure 2 indicates that the intraseasonal forecast skill of CFSv1 is the lowest among the four models with rainfall smaller than one week and U850 about two weeks. The other three models have systematically higher skills than CFSv1 with rainfall of 1–2 weeks and

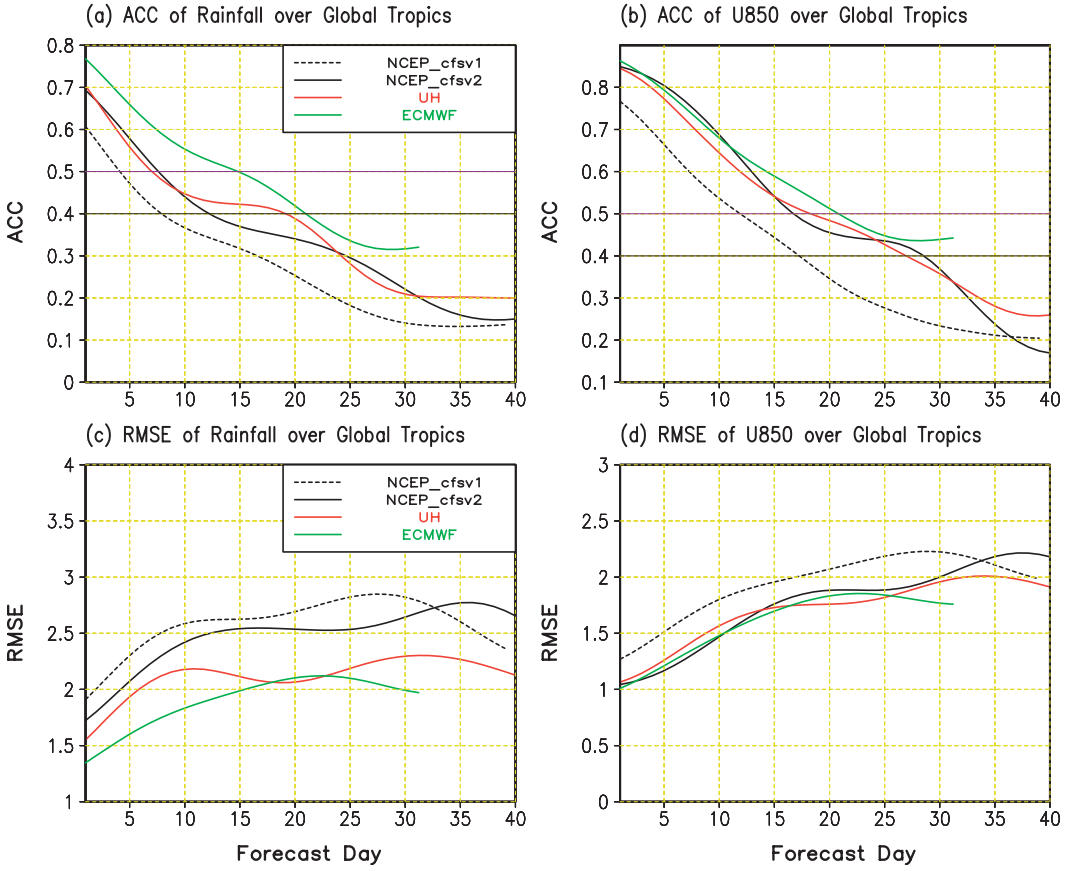


FIG. 2. The ACCs of (a) intraseasonal rainfall and (b) U850 along with (c),(d) their respective RMSEs between the observations and those forecasted by CFSv1, CFSv2, UH, and ECMWF models over the global tropics (30°S–30°N) as a function of forecast lead time (days).

U850 of 2–3 weeks (Fig. 2a). The ECMWF model is the best among all four particularly for rainfall.

The higher skills of ECMWF, CFSv2, and UH over CFSv1 are partly attributed to better initial conditions, which can be seen from the larger ACCs at initial time for the first three models (Figs. 2a,b). Because the ERA-Interim, CFSR, FNL, and NCEP R2 data have been used by ECMWF, CFSv2, UH, and CFSv1, respectively, as initial conditions, the initial ACC differences are actually consistent with the findings of Wang et al. (2012) that the representations of tropical intraseasonal variability in CFSR and ERA-Interim are much better than that in the NCEP R2. The initial dynamical fields are almost the same among ECMWF, UH, and CFSv2 (Fig. 2b). Superior initial rainfall skill of ECMWF over that of CFSv2 and UH (Fig. 2a) is likely because of the explicit assimilation of observed rain rate into ERA-Interim (Simmons et al. 2007).

The seasonal-mean RMSEs of forecasted rainfall and U850 are also given in Figs. 2c and 2d. The results are consistent with those measured with the ACCs. The forecasts of the CFSv1 have larger RMSEs for both rainfall and U850 than the other three models. As for the ACCs (Fig. 2b), the initial RMSEs of U850 in ECMWF, CFSv2, and UH are almost the same (Fig. 2d). For forecasted rainfall (Fig. 2c), however, ECMWF has the smallest RMSEs, followed by UH and CFSv2.

### b. *CFSv2 versus UH*

A more detailed comparison of the forecasts between the CFSv2 and UH models has been given in this subsection. Because both models use very similar initial conditions (Figs. 2a,b), different behaviors of the forecasts shed light on the strengths and weaknesses of each model for this specific year. The finding from this analysis may also provide useful guidance on the use of intraseasonal forecasts from these models. The forecast skills of CFSv2 and UH (Fig. 3) have a nearly opposite variation as a function of initial dates. On the occasions when the skill of CFSv2 is low, the skill of UH is high, and vice versa. This is very obvious for the 850-hPa zonal wind (Figs. 3c,d). Figure 3c indicates that CFSv2 has

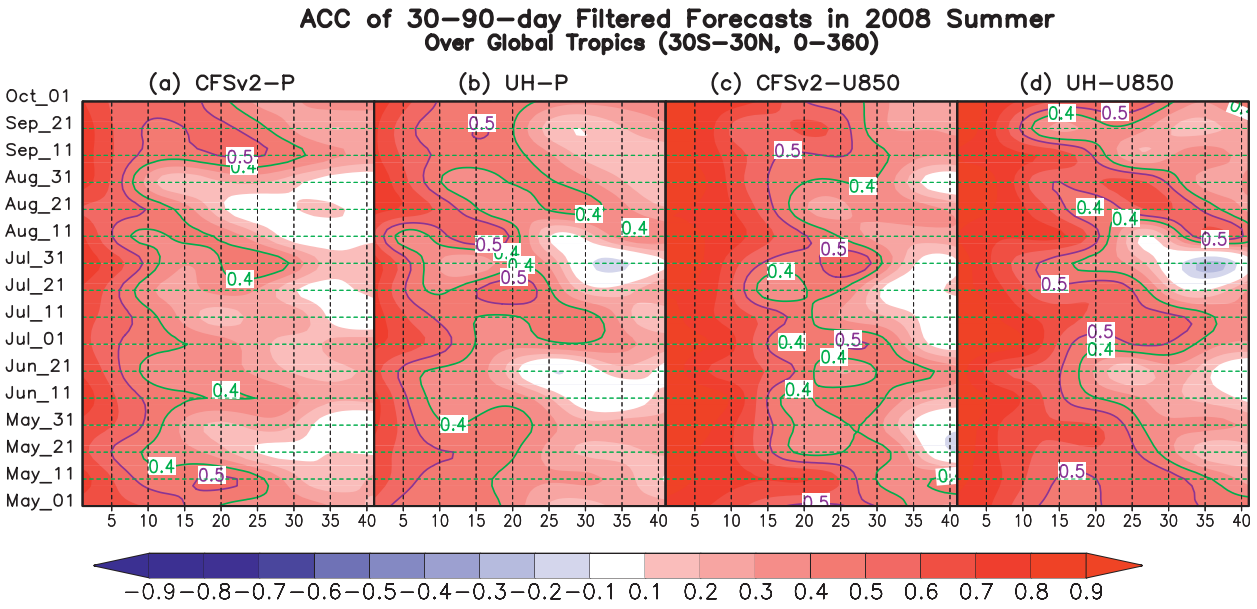


FIG. 3. The ACCs between forecasted and observed rainfall or U850 over the global tropics in the summer 2008 as a function of initial dates (ordinate axis): (a) skill of forecasted rainfall by CFSv2, (b) skill of forecasted rainfall by UH, (c) skill of forecasted U850 by CFSv2, and (d) skill of forecasted U850 by UH on different lead days (abscissa axis).

relatively lower skill around 31 May, 11 July, and 21 August, while UH has relatively higher skill around these dates (Fig. 3d). On the other hand, when UH has lower skill around 21 June, 31 July, and 11 September, the skill of CFSv2 is relatively higher. A similar situation exists for rainfall (Figs. 3a,b). For example, the skill of CFSv2 is very low around 31 May, 11 July, and 31 August (Fig. 3a), but the skill of UH around these dates is relatively high (Fig. 3b). When UH skill is low around 21 June, 31 July, and 11 September, CFSv2 has relatively high skill.

To understand why these two models have opposite skill variations (Figs. 3a,b), two cases are selected for further analysis. They are forecasts initialized on 31 July and 31 August. For the first case, CFSv2 has much higher skill than UH. For the second case, the skill of UH is much higher than that of CFSv2. Figure 4 compares the forecasted rainfall anomalies from CFSv2 and UH initialized on 31 July. Initially, a dipole pattern exists over the Indian sector (Figs. 4a,f) with a positive convective belt around 15°N and a negative convective belt near the equator. For the UH forecast at day 10 (Fig. 4h), the northern convective belt weakens considerably and a fictitious convection develops near the equator, while CFSv2 is still able to maintain the initial dipole pattern as in the observations (Fig. 4c). The onset of the near-equatorial convection in CFSv2 occurs 10 days later and agrees very well with the observations (Fig. 4d). Toward day 30, the initial dipole pattern has reversed sign with a positive (negative) rainfall anomaly near the equator (around 15°N), which has been well reproduced by CFSv2 (Fig. 4e). However, the near-equatorial convection in the UH forecast (Figs. 4h,i) has already been replaced with a suppressed phase (Fig. 4j). This result indicates that for the five intraseasonal events that occurred in the summer 2008, if the initial convection is near the Asian summer monsoon trough, then the UH model tends to produce an early false onset in the equatorial Indian Ocean, resulting in much lower skill than that of CFSv2.

The forecasts initialized on 31 August, however, suggest that when the initial convection is near the equator along with a suppressed phase in the monsoon trough, the UH model has much higher skill than CFSv2 (Fig. 5). For the first-day forecasts (Figs. 5a,f), a convective rain belt exists near the equator, which extends from the western Indian Ocean to western Pacific Ocean. For CFSv2, the near-equatorial eastward-propagating convection decays too fast, resulting in the Maritime Continent being largely covered by a negative anomaly in as early as 5 and 10 days (Fig. 5c). The northward propagation of the convection is also very slow and tends to hang around 10°N over the northwest Indian Ocean (Figs. 5b–e). On the other hand, the UH model reproduces the observed near-equatorial eastward and northward propagations in the Indian Ocean and western Pacific sectors very well (Figs. 5g–j). A tilted rain belt from the eastern Arabian Sea to the Maritime Continent forms on day 10 and gradually moves northward. Contrary to CFSv2, the forecasted rainfall anomaly in the UH model

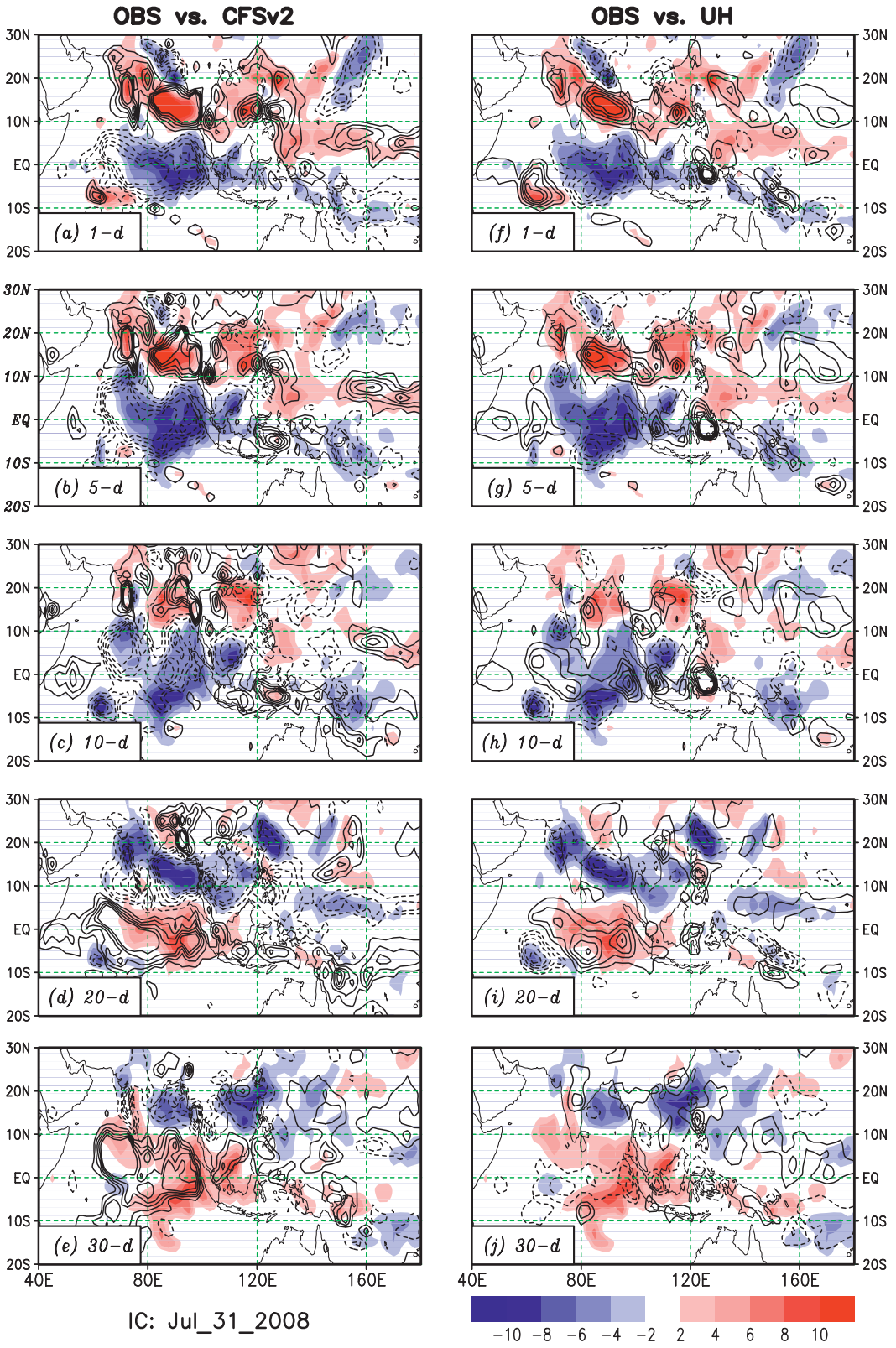


FIG. 4. (a)–(j) Observed (shading) and forecasted (contours; CI is 2 mm day$^{-1}$ with the zero contour line excluded) intraseasonal rainfall anomalies (mm day$^{-1}$) by the CFSv2 and UH models initialized on 31 Jul 2008. Solid (dashed) contours represent positive (negative) anomalies.

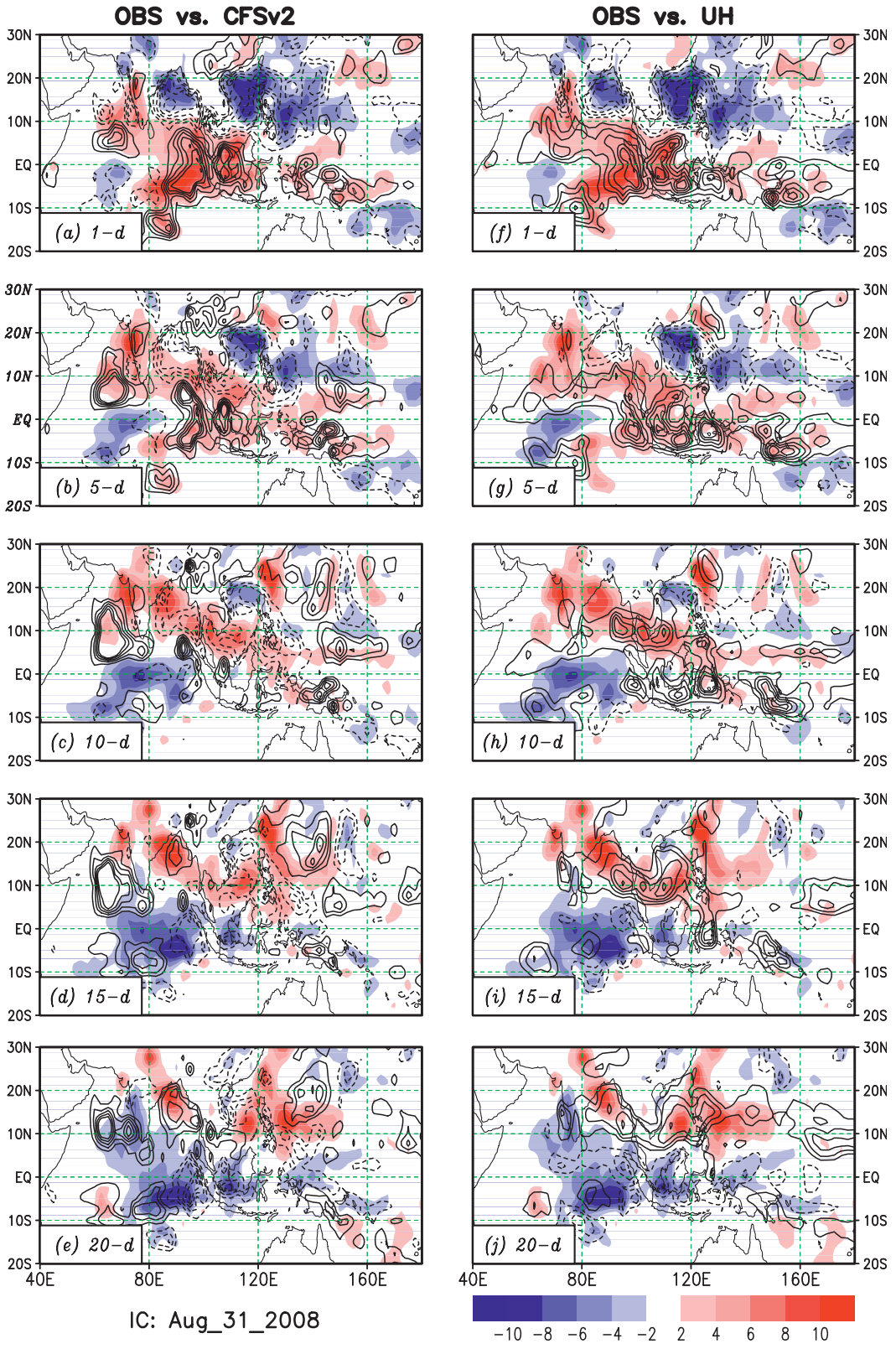


FIG. 5. As in Fig. 4, but for 31 Aug 2008.

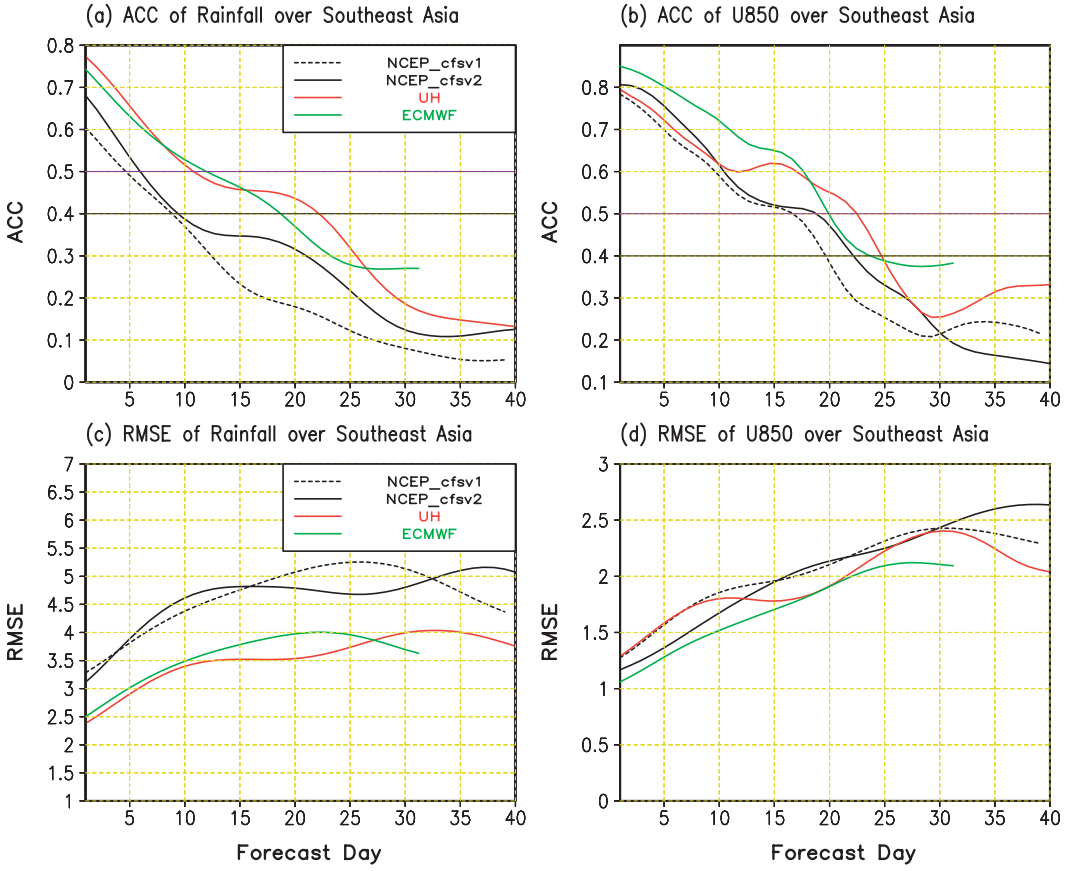


FIG. 6. ACCs of (a) intraseasonal rainfall and (b) U850 along with (c),(d) their respective RMSEs between the observations and those forecasted by CFSv1, CFSv2, UH, and ECMWF models over Southeast Asia (10°–30°N, 60°–120°E) as a function of the forecast lead time (days).

is still positive over the Maritime Continent on days 5 and 10 (Figs. 5g,h). When positive rainfall anomalies gradually move out, negative anomalies start to set into the Indian Ocean as in the observations (Figs. 5i,j).

## 4. Intraseasonal forecast skill over Southeast Asia

As shown by many previous studies (e.g., Lau and Chan 1986; Kemball-Cook and Wang 2001; Sobel et al. 2010), the largest convective variance of tropical intraseasonal variability during boreal summer is present in four oceanic basins: the equatorial and northern Indian Ocean, the South China Sea, the western North Pacific, and the eastern North Pacific. Tropical intraseasonal variability significantly modulates the occurrences of monsoon depressions and tropical cyclones in these regions, which offers an opportunity for extended-range probabilistic forecasting of these extreme events and provides early warning to the affected maritime and coastal activities (e.g., Vitart et al. 2010; Fu and Hsu 2011; Belanger et al. 2012). The northward-propagating BSISO, therefore, can impact the weather activities over Southeast Asia directly by inducing active and break spells and indirectly by modulating tropical cyclones and monsoon depressions in the northern Indian Ocean, South China Sea, and western North Pacific. The intraseasonal forecasting capability of the four models in this extended Southeast Asian domain (10°–30°N, 60°–120°E) is examined in this section.

Figure 6 summarizes the seasonal-mean skills of rainfall and U850 in the summer 2008 over Southeast Asia for the four models. The ECMWF and UH models have similar skill in this region for both rainfall and U850. The mean rainfall forecast skill measured by the ACC is slightly more than one week (Fig. 6a); the skill of U850 is around three weeks (Fig. 6b). The results from the RMSE measurements (Figs. 6c,d) are consistent with the ACC. Although the skill of CFSv2 in this area is also consistently higher than that of CFSv1, the improvement is not as large as that over the global tropics. Similar results can be seen from the RMSE measurements (Figs. 6c,d).

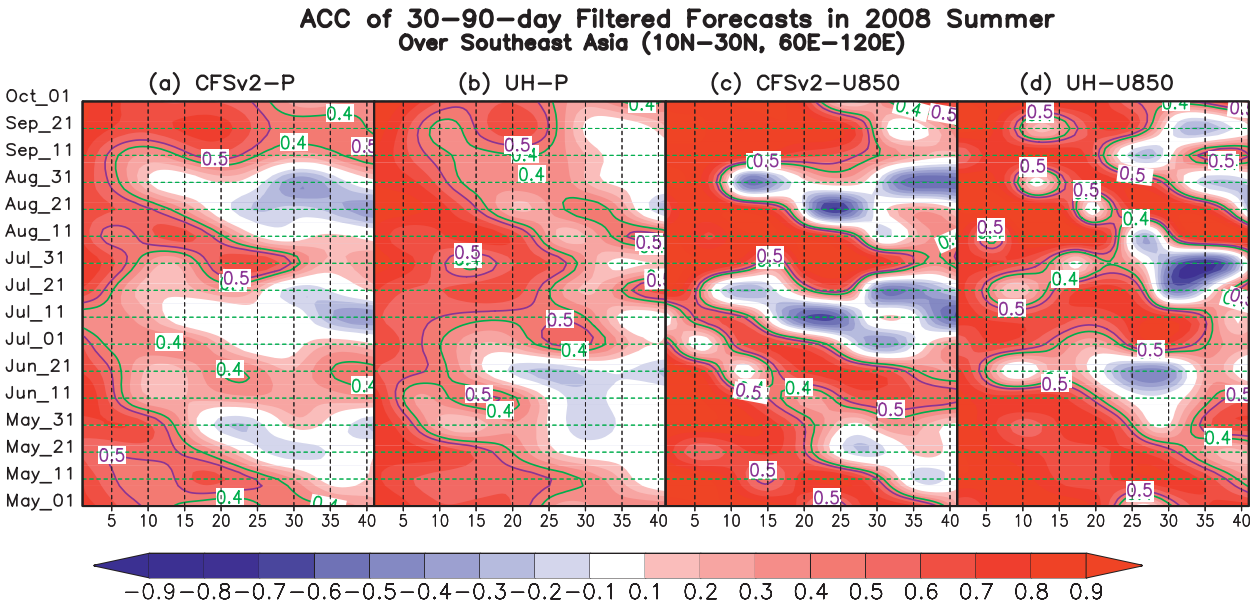


FIG. 7. ACCs between the forecasted and observed rainfall or U850 over Southeast Asia (10°–30°N, 60°–120°E) in the summer 2008 as a function of initial dates: (a) skill of forecasted rainfall by CFSv2, (b) skill of forecasted rainfall by UH, (c) skill of forecasted U850 by CFSv2, and (d) skill of forecasted U850 by UH.

As in the global tropics, the skills of the CFSv2 and UH models over Southeast Asia (Fig. 7) also exhibit significant fluctuations at different initial dates. For CFSv2 (Figs. 7a,c), there are apparently four pulses representing higher skill with three low-skill periods in between for both rainfall and U850. Referring back to the northward-propagating intraseasonal events that occurred in this year (Fig. 1b), we found that the four periods with higher skill correspond to initial convection over Southeast Asia (between 10° and 30°N). This suggests that the model reproduces the active-to-break monsoon transitions well for these cases. The three low-skill periods correspond to an initially suppressed monsoon over Southeast Asia, which indicates that the forecasts have difficulty reproducing break-to-active monsoon transitions. Similar to the situation over the global tropics (Fig. 3), for these cases the temporal skill variations between CFSv2 and UH have an out-of-phase tendency for the U850 (Figs. 7c,d) but are not so obvious for rainfall (Figs. 7a,b). For example, the forecast skill in the UH model (Fig. 7b) is very high from July to October, while the CFSv2 model has two obvious skill dips during the same period (Fig. 7a; e.g., the forecasts initialized on 11 July and 31 August, which correspond to break-to-active monsoon transitions). The cases examined in this study hint that, for CFSv2 over Southeast Asia, the active-to-break monsoon transition is much more predictable than the other way around, which is consistent with the observational study of Goswami and Xavier (2003). Future study with long-term hindcasts is needed to examine to what degree this is a general characteristics of the model.

To further understand the cause of the CFSv2 skill dip on 11 July (Fig. 7), the forecasted and observed rainfall anomalies averaged between 60° and 120°E from 20°S to 30°N are given in Fig. 8. A northward-propagating intraseasonal event occurred during the forecast period. If we only focus on the near-equatorial region (e.g., between 10°S and 5°N), the forecast of CFSv2 is very good, which captures the development of an active phase and the transition to a break phase around late July. The model is even able to predict the initiation of a new event one month later (Figs. 8a,b). If we turn to Southeast Asia (north of 10°N), the observed northward-propagating event brings a wet period there from late July to early August. The forecasted rain belt, however, tends to hang around 10°N instead of the observed 17°N (Figs. 8a,b). The factors that hinder the continuous northward progression of the rain belt in the model warrant further study. The relatively higher skill of the UH model on 11 July (Fig. 7) can be attributed to the better representation of this northward-propagating event in the model (Figs. 8c,d).

The ECMWF model has a very similar seasonal-mean forecast skill to the UH model over Southeast Asia (Fig. 6), as does its skill variations as a function of initial dates (Fig. 9). As in the UH model (Fig. 7), a drastic skill plunge occurs in June and a small dip appears in late August and early September. The relatively lower skill in June is

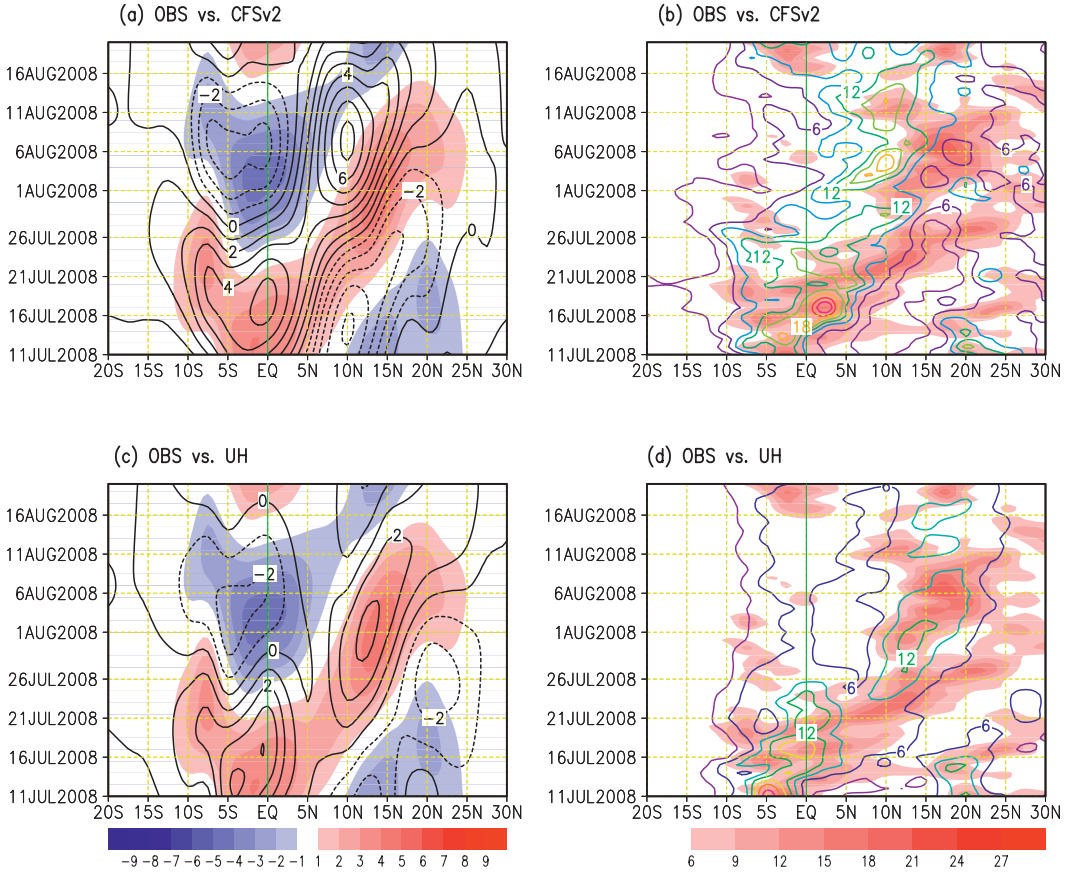


FIG. 8. Time–latitude cross sections of observed (shading) and forecasted (contours) (a),(c) intraseasonal rainfall anomalies (CI is 1 mm day$^{-1}$) and (b),(d) total amount (CI is 3 mm day$^{-1}$) averaged over 60°–120°E. Here (a) and (b) are forecasts from CFSv2; (c) and (d) are forecasts from UH. All forecasts are initialized on 11 Jul 2008.

attributed to a tendency to produce an early false onset of a new intraseasonal event (e.g., Fig. 10d).

Because the summer rainfall over Southeast Asia largely results from the northward-propagating intraseasonal variability (Yasunari 1979), the intraseasonal forecast skill of the Asian summer monsoon relies highly on the models' capability to represent the northward propagation of the BSISO. The relatively higher skills of the ECMWF and UH models than the CFSv2 model in the summer 2008 are primarily attributed to better representation of the northward-propagating BSISO (Fu et al. 2003; Vitart and Molteni 2009).

What are the possible causes for the lower skill during the break-to-active transition than during the active-to-break transition? In nature, the lower predictability of the break-to-active monsoon transition (Goswami and Xavier 2003) likely reflects the large interevent variations of northward-propagating intraseasonal convection in the observations (e.g., Wang et al. 2006). The higher predictability of the active-to-break monsoon transition is probably because the primary governing processes of this transition are quite deterministic. Active convection cools the boundary layer through downdrafts and warms the upper troposphere through diabatic heating release, which stabilizes the entire troposphere and leads to the decay of convection (or the transition to break phase of the monsoon). In the models, the relatively lower forecast skill of the break-to-active monsoon transition is likely because of the models' difficulty to reproduce the uniqueness of individual northward-propagating convective events. One encouraging result is that some break-to-active monsoon transitions can be well predicted (Figs. 7b, 8c, and 9a), which suggests that improved representation of northward-propagating intraseasonal oscillations may be able to alleviate the so-called monsoon prediction barrier problem to some degree.

## 5. Discussion and concluding remarks

### a. *Discussion*

Our analysis of the forecasts in the summer 2008 shows a great promise in using dynamical models to carry out

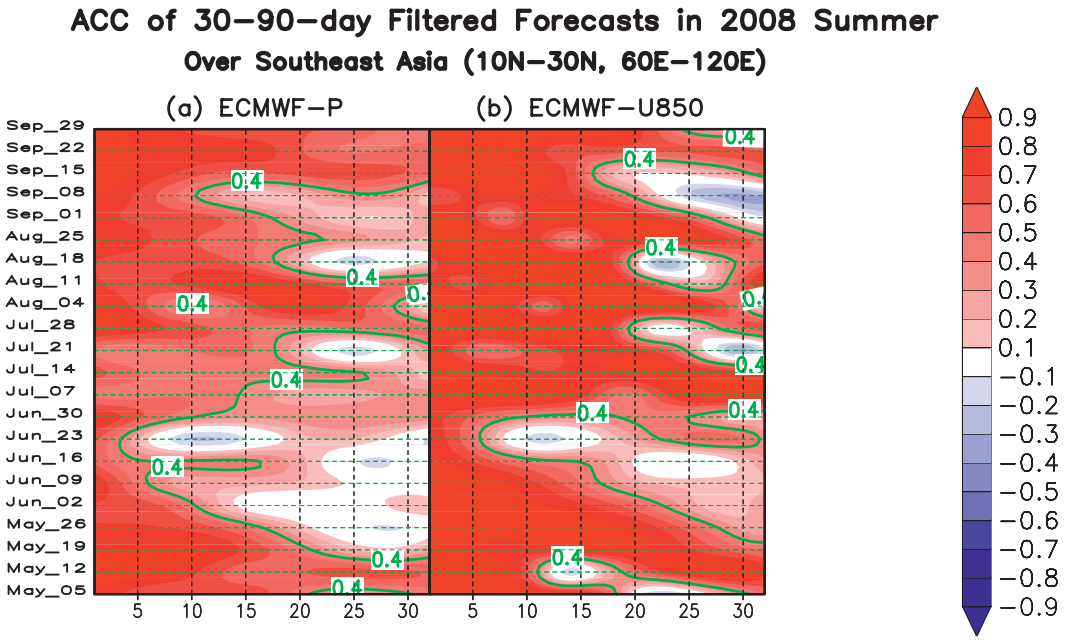


FIG. 9. ACCs between the forecasted and observed rainfall or U850 over Southeast Asia (10°–30°N, 60°–120°E) in the summer 2008 as a function of initial dates, for the skill of (a) forecasted rainfall and (b) U850 by the ECMWF.

operational intraseasonal forecasting of the Asian summer monsoon (e.g., Figs. 10a,c,e). At the same time, the practical skills of the models are still much less than their potential predictability (Fu et al. 2008; Ding et al. 2011), largely because of the models' difficulty in realistically representing individual BSISO events or possibly because the models' potential predictability is overestimated (Pegion and Sardeshmukh 2011). To facilitate further detailed diagnosis and model improvement, examples of "good" and "bad" forecasts from ECMWF, UH, and CFSv2 in the summer 2008 are highlighted here. The possible causes for the bad forecasts are discussed, which will provide useful insights for subsequent diagnosis with longer hindcasts and for the effort to improve models. However, it is well recognized that improving dynamical models takes very long cycles (Jakob 2010). With this in mind, we further explore the possibility to advance intraseasonal forecast skill by the developments of a multimodel ensemble and a combined dynamical–statistical ensemble.

### 1) POSSIBLE CAUSES OF BAD FORECASTS IN DYNAMICAL MODELS

Figure 10 highlights examples of good and bad forecasts of monsoon intraseasonal events from UH, ECMWF, and CFSv2 based on the skill estimates in Figs. 7 and 9. The good example for the UH model is the forecast initialized on 21 July (Fig. 10a) that reproduces the northward-propagating wet phase well and maintains it toward early August, even including the reinitiation of a new intraseasonal event near the equator in mid-August. For the ECMWF model, the forecast initialized on 11 August (Fig. 10c) captures the monsoon active-to-break transition and the reinitiation and northward propagation of a new event. For CFSv2, the forecast initialized on 31 July with initial convection in the monsoon trough (~15°N) predicts the gradually northward-propagating rain belt and the reinitiation of a new event near the equator well (Fig. 10e).

The bad examples for both the UH (Fig. 10b) and ECMWF models (Fig. 10d) are the early false onsets of new intraseasonal events. For CFSv2, it is the forecast with initial convection near the equator and very slow northward propagation of the convection (Fig. 10f). The early false onset problems in the UH and ECMWF models are first revealed in this study through intercomparison of forecasts. This type of problem is very difficult to detect through diagnosing long-term free simulations. On the other hand, the slow propagation of intraseasonal variability in the CFS models has been detected from the diagnoses of free simulations and forecasts (Pegion and Kirtman 2008; W. Wang et al. 2009; Achuthavarier and Krishnamurthy 2011; Weaver et al. 2011). By analyzing the monsoon intraseasonal oscillation in CFSv2, B. Goswami et al. (2012, unpublished manuscript) showed that while CFSv2 reproduces the

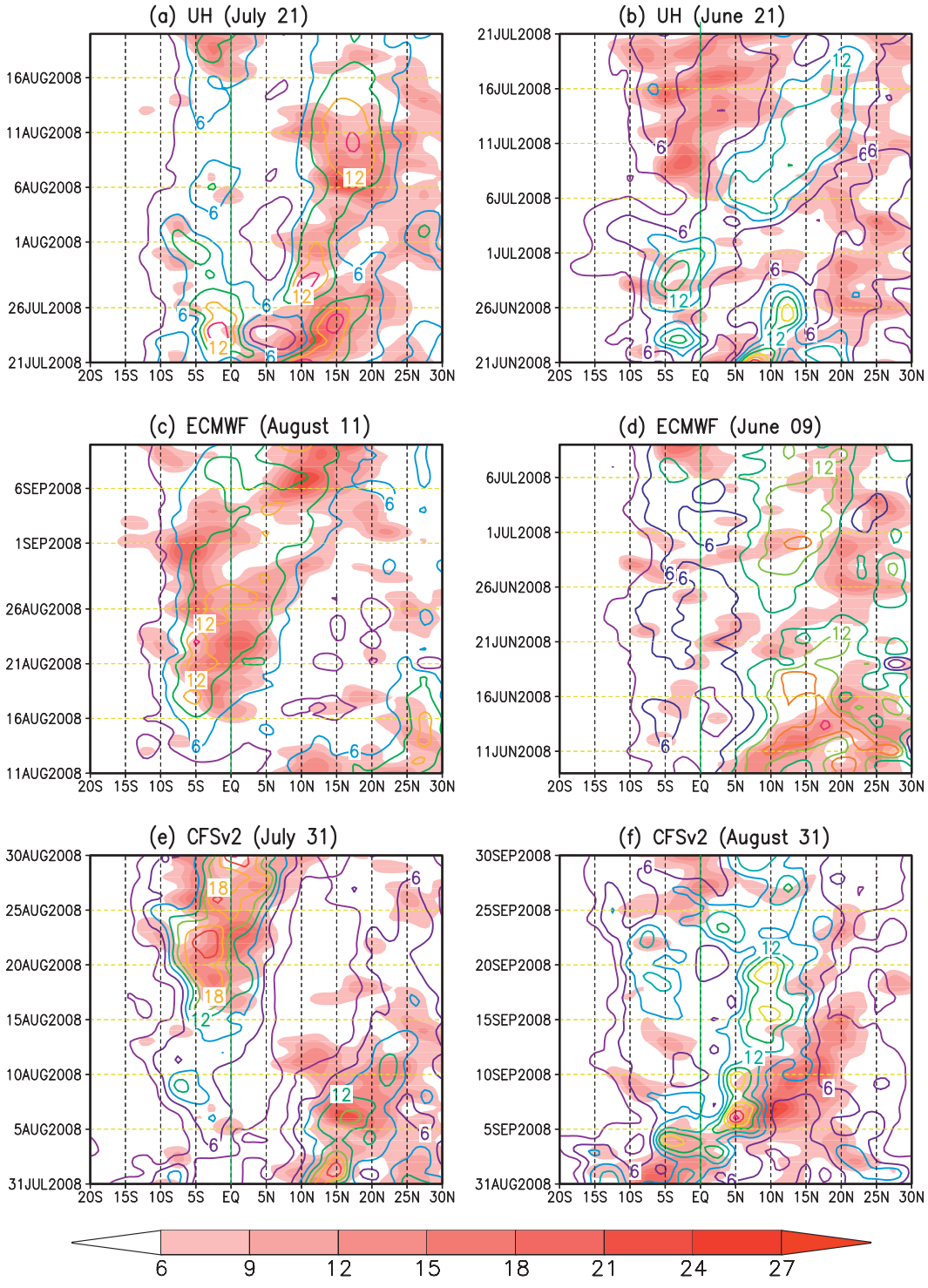


FIG. 10. Examples of (left) "good" intraseasonal monsoon forecasts and (right) "bad" forecasts, from the (a),(b) UH, (c),(d) ECMWF, and (e),(f) CFSv2 in the summer 2008. All results are presented as time–latitude cross sections of total rainfall (mm day$^{-1}$) averaged over 60°–120°E. Observations (forecasts) are in shading (contours; CI is 3 mm day$^{-1}$).

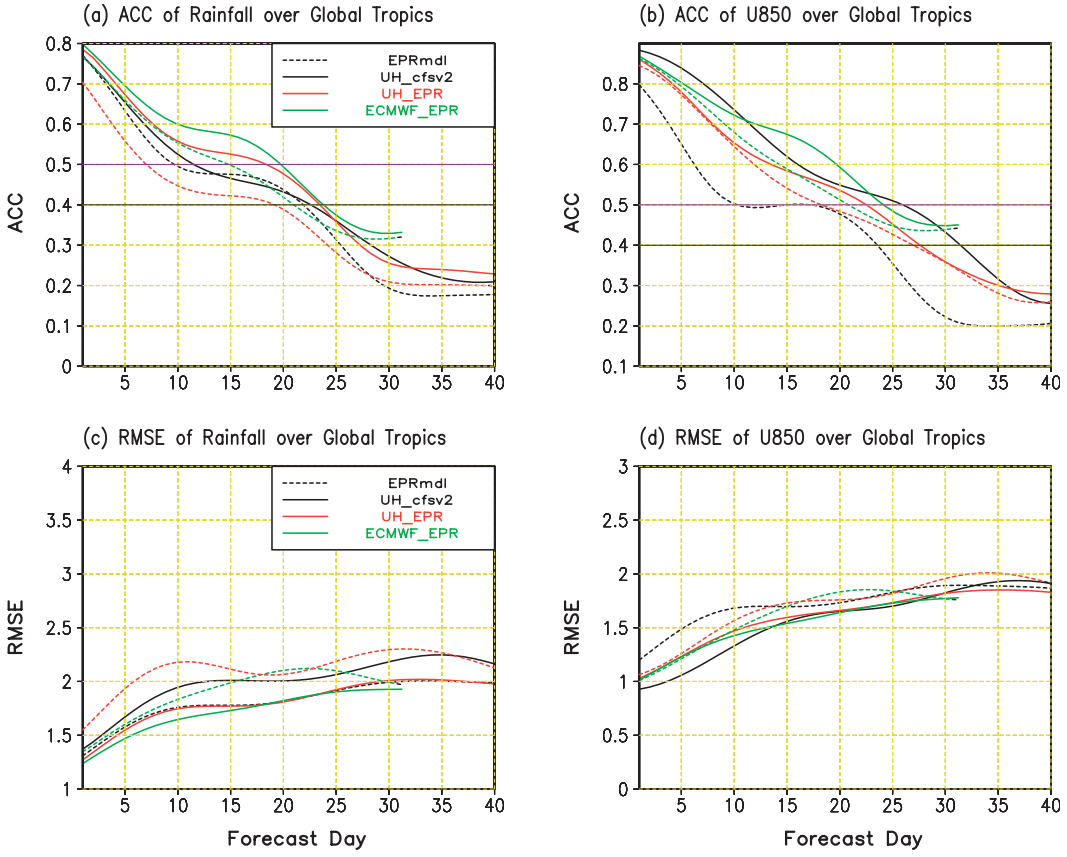


FIG. 11. ACCs of (a) intraseasonal rainfall and (b) U850 along with (c),(d) their respective RMSEs between the observations and those forecasted by EPRmdl, multimodel ensemble CFSv2_UH, UH_EPRmdl ensemble, and ECMWF_EPRmdl ensemble over the global tropics (30°S–30°N) as a function of forecast lead time in days. Results from the ECMWF alone (dashed green lines) and UH alone (dashed red lines) have been repeated here for reference.

overall observed characteristics of north–south space–time spectra of rainfall anomalies over 20°S–35°N between 70° and 90°E during June–September, the wavenumber-1 power spectrum maximum of the northward component is around the period of 61 days in CFSv2 relative to 40 days in the observation, indicating that the northward propagation in CFSv2 is too slow.

Preliminary diagnosis (not shown) suggests that the early false BSISO onsets in UH and ECMWF are related to the rapid development of tropical cyclone–like disturbances in these two models. For the UH model, the false tropical cyclones frequently occur just south of the equatorial Indian Ocean, probably leading to the early false BSISO onset as seen in Fig. 10b. For the ECMWF model, frequent false tropical cyclones tend to appear over the Arabian Sea and Bay of Bengal (Belanger et al. 2012), likely contributing to the early false BSISO onset as seen in Fig. 10d. This hypothesis is obtained from a very limited case study. Further diagnostic and modeling studies with more cases and detailed analysis are needed to address this issue, which is beyond the scope of the present study. The slow northward propagation in CFSv2 is probably related to the misrepresentations of the cumulus parameterization and air–sea coupling. Seo and Wang (2010) found that the slow propagation of intraseasonal variability in CFSv1 can be significantly improved by replacing its default cumulus parameterization with a new scheme from increased stratiform rainfall (Fu and Wang 2009). The sensitivity experiments of W. Wang et al. (2009) suggest that improved air–sea coupling in CFSv1 will lead to much better northward-propagating BSISO.

### 2) DEVELOPMENTS OF MULTIMODEL AND DYNAMICAL–EMPIRICAL ENSEMBLES

Given the problems of state-of-the-art dynamical models and long cycles needed to improve the models, additional methods have been sought to enhance and/or supplement the dynamical prediction. Practical approaches include the developments of multimodel ensembles

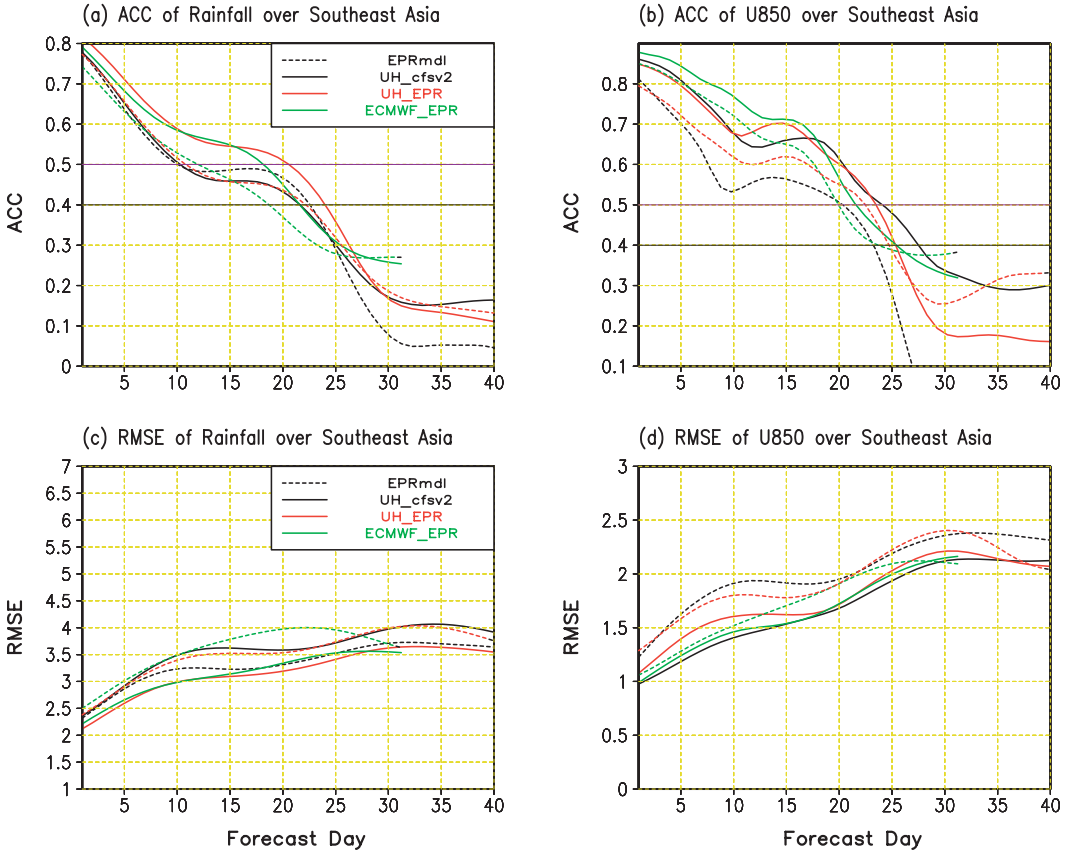


FIG. 12. As in Fig. 11, but for Southeast Asia (10°–30°N, 60°–120°E).

(Krishnamurti et al. 1999; B. Wang et al. 2009) and empirical models (Waliser et al. 1999; Wheeler and Weickmann 2001; Goswami and Xavier 2003; Jones et al. 2004; Jiang et al. 2008). Likely because of the complementary nature between CFSv2 and UH, an equal-weighted ensemble with these two models results in a skill increase of BSISO-related rainfall from one (Fig. 2a) to two weeks (Fig. 11a) over the global tropics; so does the skill of 850-hPa zonal wind (Fig. 11b). Along with the skill increase measured with ACCs, the RMSEs of the ensemble (Figs. 11c,d) are also systematically reduced in comparison with that of individual models (Figs. 2c,d). However, the ensemble does not increase the skill of BSISO-related rainfall over Southeast Asia (Figs. 12a,c) although the skill of 850-hPa zonal wind is significantly extended in comparison with that of individual models (Figs. 12b,d). The reasons for this behavior deserve further study. Because the initial dates of the ECMWF forecasts are different from the UH model, no multimodel ensemble with the ECMWF has been attempted.

Following the approach of Wheeler and Weickmann (2001), a simple empirical model (EPRmdl) has been developed to generate intraseasonal forecasting of rainfall and U850 anomalies for the summer 2008. The skill of EPRmdl reaches the same level as CFSv2, UH, and ECMWF for BSISO-related rainfall but is systematically lower than dynamical models for U850 over the global tropics and Southeast Asia (Figs. 11b and 12b). When equal-weighted ensembles are developed with either the UH/EPRmdl pair or the ECMWF/EPRmdl pair, the resultant skills of BSISO-related rainfall (U850) reach three weeks (beyond) over the global tropics and Southeast Asia (Figs. 11 and 12). These results demonstrate that the developments of both multimodel and dynamical–empirical ensembles are fruitful pathways to advance the practical intraseasonal forecast skill of the Asian summer monsoon.

### *b. Concluding remarks*

In this study, we assessed the intraseasonal forecast skills of rainfall and 850-hPa zonal wind over the global tropics and Southeast Asia for the summer 2008 in four state-of-the-art operational and research models: NCEP CFS, versions 1 and 2; UH; and ECMWF (Figs. 2 and 6). The CFSv1 model has the lowest skill among the four. The other three models have similar skill, with ECMWF

being the best. The forecast skills of the models vary considerably with initial conditions. The skill fluctuations of UH and ECMWF are very similar. Both of them are almost opposite with that of CFSv2. The possible link between skill variations and model problems has been explored. We also attempt to advance intraseasonal forecast skill by the developments of multimodel and dynamical–empirical ensembles.

One major metric used to quantify the intraseasonal forecast skill in this study is the spatial anomaly correlation coefficient, which measures the similarity of the spatial patterns between the forecasts and observations. Rainfall has been selected as a key predictand in this study because it can be directly utilized by end users for the purposes of agricultural planning, water management, and disaster prevention. Following the convention in measuring weather forecast skill, an ACC criterion of 0.5 has been used here to define the intraseasonal forecast skill, which is higher than that used in previous studies (e.g., Jones et al. 2000; Lin et al. 2008; Fu et al. 2011). The resultant skill of rainfall (U850) over the global tropics is about 1–2 weeks (3 weeks) for the ECMWF, UH, and CFSv2 models (Fig. 2). The skill of the CFSv1 model is much lower than the other three.

Over the global tropics, CFSv2 has higher skill than CFSv1 partly because of better initial conditions (Fig. 2; see also Wang et al. 2012; Weaver et al. 2011). The CFSv2 and UH models are complementary to each other in terms of an out-of-phase skill fluctuations with different initial conditions in the summer 2008 (Fig. 3). For the cases when initial convection is located in the monsoon trough (~15°N), CFSv2 has much higher skill than UH (Fig. 3) because the UH model at this time tends to produce an early false onset in the equatorial Indian Ocean (Fig. 4). For cases when initial convection is near the equator, CFSv2 has much lower skill than UH (Fig. 3) because of the slow northward propagation of BSISO in CFSv2 (Fig. 5).

Over Southeast Asia, the intraseasonal forecast skill of the monsoon rainfall (U850) is also about 1–2 weeks (3 weeks) for all four models (Fig. 6). In this region, intraseasonal forecast skill is largely determined by a model's ability to represent the northward-propagating BSISO. The relatively lower skill of CFSv1/CFSv2 (Fig. 6a) for BSISO events that occur in the summer 2008 is primarily because of the difficulty of realistically representing the northward propagation, which is particularly severe during the break-to-active monsoon transition rather than the active-to-break transition. This characteristic of monsoon predictability asymmetry was first revealed from the observational study of Goswami and Xavier (2003). The break-to-active transition, therefore, has been referred to as the ''monsoon prediction barrier.'' It is also encouraging to note that with improved representation of the northward-propagating BSISO (Fig. 8), this monsoon prediction barrier problem can be alleviated to some degree for the limited number of cases investigated in this study (Figs. 7 and 9).

Our analysis based on summer 2008 forecasts suggests that early false BSISO onset in the UH and ECMWF models and slow northward propagation in the CFSv2/CFSv1 models are potentially important stumbling blocks for the further advancement of intraseasonal forecasting in these models. However, because our results are based on a single summer consisting of five intraseasonal events, they do not fully represent the scope of potential issues impacting improving intraseasonal forecasting. Hypotheses of possible causes of these problems are also raised from our preliminary analysis and previous studies. Considering the limited cases used in this study, future research with long-term hindcasts and more detailed diagnosis are definitely needed. A multimodel ensemble and a dynamical–empirical ensemble are also developed. Both approaches result in much higher skill than that of the individual models (Figs. 11 and 12). This finding suggests that based on these cases in order to pursue further advancement of intraseasonal forecasting, efforts to develop both dynamical models and empirical models are necessary.

*Acknowledgments.* This work was sponsored by NOAA (NA11OAR4310096 and NA10OAR 4310247) and National Science Foundation (AGS-1005599), and by the Japan Agency for Marine-Earth Science and Technology (JAMSTEC), NASA, and NOAA through their supports of the IPRC. Additional supports are from the Asia-Pacific Economic Commission (APEC) Climate Center and China Meteorological Administration (CMA) project (GYHY201206016). Comments from four anonymous reviewers greatly helped improve the manuscript.

## REFERENCES

Achuthavarier, D., and V. Krishnamurthy, 2011: Role of Indian and Pacific SST in Indian summer monsoon intraseasonal variability. *J. Climate,* **24,** 2915–2930.

Bechtold, P., M. Kohler, T. Jung, F. Doblas-Reyes, M. Leutbecher, M. J. Rodwell, F. Vitart, and G. Balsamo, 2008: Advances in simulating atmospheric variability with the ECMWF model: From synoptic to decadal time-scales. *Quart. J. Roy. Meteor. Soc.,* **134,** 1337–1351.

Belanger, J. I., P. J. Webster, J. A. Curry, and M. T. Jelinek, 2012: Extended predictions of north Indian Ocean tropical cyclones. *Wea. Forecasting,* **27,** 757–769.

Cane, M., S. E. Zebiak, and S. C. Dolan, 1986: Experimental forecasts of El Niño. *Nature,* **321,** 827–832.

Chen, T.-C., and J. C. Alpert, 1990: Systematic errors in the annual and intraseasonal variations of the planetary-scale divergent

circulation in NMC medium-range forecasts. *Mon. Wea. Rev.,* **118,** 2607–2623.

——, and S.-P. Weng, 1999: Interannual and intraseasonal variations in monsoon depressions and their westward-propagating predecessors. *Mon. Wea. Rev.,* **127,** 1005–1020.

Ding, R., J. Li, and K.-H. Seo, 2011: Estimate of the predictability of boreal summer and winter intraseasonal oscillations from observations. *Mon. Wea. Rev.,* **139,** 2421–2438.

Fu, X., and B. Wang, 2009: Critical roles of the stratiform rainfall in sustaining the Madden–Julian oscillation: GCM experiments. *J. Climate,* **22,** 3939–3959.

——, and P. Hsu, 2011: Extended-range ensemble forecasting of tropical cyclogenesis in the northern Indian Ocean: Modulation of Madden–Julian oscillation. *Geophys. Res. Lett.,* **38,** L15803, doi:10.1029/2011GL048249.

——, B. Wang, T. Li, and J. P. McCreary, 2003: Coupling between northward-propagating intraseasonal oscillations and sea surface temperature in the Indian Ocean. *J. Atmos. Sci.,* **60,** 1733–1753.

——, ——, D. E. Waliser, and L. Tao, 2007: Impact of atmosphere–ocean coupling on the predictability of monsoon intraseasonal oscillations. *J. Atmos. Sci.,* **64,** 157–174.

——, B. Yang, Q. Bao, and B. Wang, 2008: Sea surface temperature feedback extends the predictability of tropical intraseasonal oscillation. *Mon. Wea. Rev.,* **136,** 577–597.

——, B. Wang, Q. Bao, P. Liu, and J.-Y. Lee, 2009: Impacts of initial conditions on monsoon intraseasonal forecasting. *Geophys. Res. Lett.,* **36,** L08801, doi:10.1029/2009GL037166.

——, ——, J.-Y. Lee, W. Q. Wang, and L. Gao, 2011: Sensitivity of dynamical intraseasonal prediction skills to different initial conditions. *Mon. Wea. Rev.,* **139,** 2572–2592.

Goswami, B. N., and P. K. Xavier, 2003: Potential predictability and extended range prediction of Indian summer monsoon breaks. *Geophys. Res. Lett.,* **30,** 1966, doi:10.1029/2003GL017810.

——, R. S. Ajayamohan, P. K. Xavier, and D. Sengupta, 2003: Clustering of synoptic activity by Indian summer monsoon intraseasonal oscillations. *Geophys. Res. Lett.,* **30,** 1431, doi:10.1029/2002GL016734.

Goulet, L., and J. P. Duvel, 2000: A new approach to detect and characterize intermittent atmospheric oscillations: Application to the intraseasonal oscillation. *J. Atmos. Sci.,* **57,** 2397–2416.

Hendon, H. H., B. Liebmann, M. Newmann, J. D. Glick, and J. E. Schemm, 2000: Medium-range forecast errors associated with active episodes of the Madden–Julian oscillation. *Mon. Wea. Rev.,* **128,** 69–86.

Hoyos, C. D., and P. J. Webster, 2007: The role of intraseasonal variability in the nature of Asian monsoon precipitation. *J. Climate,* **20,** 4402–4424.

Jakob, C., 2010: Accelerating progress in global atmospheric model development through improved parameterizations: Challenges, opportunities, and strategies. *Bull. Amer. Meteor. Soc.,* **91,** 869–875.

Jiang, X., D. E. Waliser, M. C. Wheeler, C. Jones, M.-I. Lee, and S. D. Schubert, 2008: Assessing the skill of an all-season statistical forecast model for the Madden–Julian oscillation. *Mon. Wea. Rev.,* **136,** 1940–1956.

Jones, C., D. E. Waliser, J.-K. E. Schemm, and W. K. M. Lau, 2000: Prediction skill of the Madden and Julian oscillation in dynamical extended range forecasts. *Climate Dyn.,* **16,** 273–289.

——, L. M. V. Carvalho, R. W. Higgins, D. E. Waliser, and J.-K. E. Schemm, 2004: A statistical forecast model of tropical intraseasonal convective anomalies. *J. Climate,* **17,** 2078–2095.

Jung, T., and Coauthors, 2012: High-resolution climate simulations with the ECMWF model in Project Athena: Experimental design, model climate, and seasonal forecast skill. *J. Climate,* **25,** 3155–3172.

Kemball-Cook, S., and B. Wang, 2001: Equatorial waves and air–sea interaction in the boreal summer intraseasonal oscillation. *J. Climate,* **14,** 2923–2942.

Kikuchi, K., B. Wang, and H. Fudeyasu, 2009: Genesis of tropical cyclone Nargis revealed by multiple satellite observations. *Geophys. Res. Lett.,* **36,** L06811, doi:10.1029/2009GL037296.

Krishnamurti, T. N., 1971: Tropical east–west circulations during the northern summer. *J. Atmos. Sci.,* **28,** 1342–1347.

——, M. Subramaniam, G. Daughenbaugh, D. Oosterhof, and J. H. Xue, 1992: One-month forecast of wet and dry spells of the monsoon. *Mon. Wea. Rev.,* **120,** 1191–1223.

——, C. M. Kishtawal, T. LaRow, D. Bachiochi, Z. Zhang, C. E. Williford, S. Gadgil, and S. Surendran, 1999: Improved weather and seasonal climate forecasts from multimodel superensemble. *Science,* **285,** 1548–1550.

Lau, K.-M., and P. H. Chan, 1986: Intraseasonal and interannual variations of tropical convection: A possible link between 40–50-day oscillation and ENSO? *J. Atmos. Sci.,* **45,** 506–521.

——, and F. C. Chang, 1992: Tropical intraseasonal oscillation and its prediction by the NMC operational model. *J. Climate,* **5,** 1365–1378.

——, and D. E. Waliser, Eds., 2012: *Intraseasonal Variability of the Atmosphere–Ocean Climate System.* 2nd ed. Springer, 613 pp.

Lee, J.-Y., and Coauthors, 2010: How are seasonal prediction skills related to models' performance on mean state and annual cycle? *Climate Dyn.,* **35,** 267–283.

——, B. Wang, M. Wheeler, X. Fu, D. Waliser, and I.-S. Kang, 2013: Real-time multivariate indices for the boreal summer intraseasonal oscillation over the Asian summer monsoon region. *Climate Dyn.,* **40,** 493–509, doi:10.1007/s00382-012-1544-4.

Liebmann, B., H. H. Hendon, and J. D. Glick, 1994: The relationship between tropical cyclones of the western Pacific and Indian Oceans and the Madden–Julian oscillation. *J. Meteor. Soc. Japan,* **72,** 401–412.

Liess, S., D. E. Waliser, and S. D. Schubert, 2005: Predictability studies of the intraseasonal oscillation with the ECHAM5 AGCM. *J. Atmos. Sci.,* **62,** 3320–3336.

Lin, H., G. Brunet, and J. Derome, 2008: Forecast skill of the Madden–Julian oscillation in two Canadian atmospheric models. *Mon. Wea. Rev.,* **136,** 4130–4149.

Lin, J.-L., and Coauthors, 2006: Tropical intraseasonal variability in 14 IPCC AR4 climate model. Part I: Convective signals. *J. Climate,* **19,** 2665–2690.

Lorenz, E. N., 2006: Predictability—A problem partly solved. *Predictability of Weather and Climate,* T. Palmer and R. Hagedorn, Eds., Cambridge University Press, 40–58.

Madden, R. A., and P. R. Julian, 1971: Detection of a 40-50 day oscillation in the zonal wind in the tropical Pacific. *J. Atmos. Sci.,* **28,** 702–708.

Matsueda, M., and H. Endo, 2011: Verification of medium-range MJO forecasts with TIGGE. *Geophys. Res. Lett.,* **38,** L11801, doi:10.1029/2011GL047480.

Matthews, A. J., 2008: Primary and successive events in the Madden–Julian oscillation. *Quart. J. Roy. Meteor. Soc.,* **134,** 439–453.

Moorthi, S., H.-L. Pan, and P. Caplan, 2011: Changes to the 2011 NCEP operational MRF/AVN global analysis/forecast system. NWS Tech. Procedures Bull. 484, 14 pp. [Available online at http://www.nws.noaa.gov/om/tpb/484.htm.]

Nakazawa, T., 1986: Intraseasonal variation of OLR in the tropics during the FGGE year. *J. Meteor. Soc. Japan,* **64,** 17–34.

Pacanowski, R. C., and S. M. Griffies, 1998: MOM 3.0 manual. NOAA/GFDL, 692 pp.

Pegion, K., and B. P. Kirtman, 2008: The impact of air–sea interactions on the simulation of tropical intraseasonal variability. *J. Climate,* **21,** 6616–6635.

——, and P. D. Sardeshmukh, 2011: Prospects for improving subseasonal predictions. *Mon. Wea. Rev.,* **139,** 3648–3666.

Rashid, H. A., H. H. Hendon, M. C. Wheeler, and O. Alves, 2011: Prediction of the Madden–Julian oscillation with the POAMA dynamical prediction system. *Climate Dyn.,* **36,** 649–661.

Reichler, T., and J. O. Roads, 2005: Long-range predictability in the tropics. Part II: 30–60-day variability. *J. Climate,* **18,** 634–650.

Rienecker, M., and Coauthors, 2009: MERRA—NASA's Reanalysis: Overview of the System. [Available online at http://gmao.gsfc.nasa.gov/pubs/docs/Rienecker377.pdf.]

Roeckner, E., and Coauthors, 1996: The atmospheric general circulation model ECHAM-4: Model description and simulation of present-day climate. Max Planck Institute for Meteorology Rep. 218, 90 pp.

Saha, S., and Coauthors, 2006: The NCEP Climate Forecast System. *J. Climate,* **19,** 3483–3517.

——, and Coauthors, 2010: The NCEP Climate Forecast System Reanalysis. *Bull. Amer. Meteor. Soc.,* **91,** 1015–1057.

Seo, K.-H., and W. Wang, 2010: The Madden–Julian oscillation simulated in the NCEP Climate Forecast System model: The importance of stratiform heating. *J. Climate,* **23,** 4770–4793.

——, J.-K. E. Schemm, C. Jones, and S. Moorthi, 2005: Forecast skill of the tropical intraseasonal oscillation in the NCEP GFS dynamical extended range forecasts. *Climate Dyn.,* **25,** 265–284.

——, W.-Q. Wang, J. Gottschalck, Q. Zhang, J.-K. E. Schemm, W. R. Higgins, and A. Kumar, 2009: Evaluation of MJO forecast skill from several statistical and dynamical forecast models. *J. Climate,* **22,** 2372–2388.

Shukla, J., 1998: Predictability in the midst of chaos: A scientific basis for climate forecasting. *Science,* **282,** 728–731.

——, R. Hagedorn, B. Hoskins, J. Kinter, J. Marotzke, M. Miller, T. N. Palmer, and J. Slingo, 2009: Strategies: Revolution in climate prediction: A declaration at the world modeling summit for climate prediction. *Bull. Amer. Meteor. Soc.,* **90,** 175–178.

Simmons, A., S. Uppala, D. Dee, and S. Kobayashi, 2007: ERA-Interim: New ECMWF reanalysis products from 1989 onwards. *ECMWF Newsletter,* No. 110, ECMWF, Reading, United Kingdom, 25–35.

Sobel, A. H., E. D. Maloney, G. Bellon, and D. M. Frierson, 2010: Surface fluxes and tropical intraseasonal variability: A reassessment. *J. Adv. Model. Earth Syst.,* **2** (2), doi:10.3894/JAMES.2010.2.2.

Tiedtke, M., 1989: A comprehensive mass flux scheme for cumulus parameterization in large-scale models. *Mon. Wea. Rev.,* **117,** 1779–1800.

van den Dool, H. M., and S. Saha, 1990: Frequency dependence in forecast skill. *Mon. Wea. Rev.,* **118,** 128–137.

Vitart, F., and F. Molteni, 2009: Dynamical extended-range prediction of early monsoon rainfall over India. *Mon. Wea. Rev.,* **137,** 1480–1492.

——, S. Woolnough, M. A. Balmaseda, and A. M. Tompkins, 2007: Monthly forecast of the Madden–Julian oscillation using a coupled GCM. *Mon. Wea. Rev.,* **135,** 2700–2715.

——, and Coauthors, 2008: The new VarEPS-monthly forecasting system: A first step towards seamless prediction. *Quart. J. Roy. Meteor. Soc.,* **134,** 1789–1799.

——, A. Leroy, and M. C. Wheeler, 2010: A comparison of dynamical and statistical predictions of weekly tropical cyclone activity in the Southern Hemisphere. *Mon. Wea. Rev.,* **138,** 3671–3682.

Waliser, D. E., C. Jones, J. K. E. Schemm, and N. E. Graham, 1999: A statistical extended-range tropical forecast model based on the slow evolution of the Madden–Julian oscillation. *J. Climate,* **12,** 1918–1939.

——, W. Stern, S. Schubert, and K. M. Lau, 2003: Dynamic predictability of intraseasonal variability associated with the Asian summer monsoon. *Quart. J. Roy. Meteor. Soc.,* **129,** 2897–2925.

——, and Coauthors, 2012: The ''year'' of tropical convection (May 2008–April 2010): Climate variability and weather highlights. *Bull. Amer. Meteor. Soc.,* **93,** 1189–1218.

Wang, B., and H. Rui, 1990: Synoptic climatology of transient tropical intraseasonal convection anomalies: 1975–1985. *Meteor. Atmos. Phys.,* **44,** 43–61.

——, and X. Xie, 1997: A model for the boreal summer intraseasonal oscillation. *J. Atmos. Sci.,* **54,** 72–86.

——, P. Webster, K. Kikuchi, T. Yasunari, and Y. Qi, 2006: Boreal summer quasi-monthly oscillation in the global tropics. *Climate Dyn.,* **27,** 661–675.

——, and Coauthors, 2009: Advance and prospectus of seasonal prediction: Assessment of the APCC/CLiPAS 14-model ensemble retrospective seasonal prediction (1980–2004). *Climate Dyn.,* **33,** 93–117, doi:10.1007/S00382-008-0460-0.

Wang, J., W. Wang, X. Fu, and K.-H. Seo, 2012: Tropical intraseasonal rainfall variability in the CFSR. *Climate Dyn.,* **38,** 2191–2207, doi:10.1007/s00382-011-1087-0.

Wang, W., M. Chen, and A. Kumar, 2009: Impacts of ocean surface on the northward propagation of the boreal-summer intraseasonal oscillation in the NCEP climate forecast system. *J. Climate,* **22,** 6561–6576.

Weaver, S., W. Q. Wang, M. Chen, and A. Kumar, 2011: Representation of MJO variability in the NCEP Climate Forecast System. *J. Climate,* **24,** 4676–4694.

Wheeler, H., and K. M. Weickmann, 2001: Real-time monitoring and prediction of modes of coherent synoptic to intraseasonal tropical variability. *Mon. Wea. Rev.,* **129,** 2677–2694.

Wilks, D. S., 2005: *Statistical Methods in the Atmospheric Sciences.* 2nd ed. Elsevier, 627 pp.

Wolff, J. O., E. Maier-Raimer, and S. Legutke, 1997: The Hamburg ocean primitive equation model. Deutsches Klimarechenzentrum Tech. Rep. 13, 98 pp.

Woolnough, S. J., F. Vitart, and M. A. Balmaseda, 2007: The role of the ocean in the Madden–Julian oscillation: Implications for the MJO prediction. *Quart. J. Roy. Meteor. Soc.,* **133,** 117–128.

Yasunari, T., 1979: Cloudiness fluctuations associated with the Northern Hemisphere summer monsoon. *J. Meteor. Soc. Japan,* **57,** 227–242.

Zhang, Q., and H. van den Dool, 2012: Relative merit of model improvement versus availability of retrospective forecasts: The case of climate forecast system MJO prediction. *Wea. Forecasting,* **27,** 1045–1051.